Article

Interconnections of coal and forest fires in Siberia and Australia:

Leonid Yurganov *

Posted Date: 25 December 2023

doi: 10.20944/preprints202312.1791.v1

Keywords: wildfires; coal fires; carbon monoxide; remote sensing

Article

Interconnections of Coal and Forest Fires in Siberia and Australia: Satellite CO Measurements

Leonid Yurganov

Independent Researcher; leonid.yurganov@gmail.com

Abstract: Carbon monoxide (CO) concentrations in wildfire plumes are easily measured from satellites. This gas can be used as a proxy for carbon dioxide. Forest fires play an important role in the carbon balance and in particular the CO balance. The most likely causes of mega-fires of 2003, 2012, 2021, and 2023 in the Northern hemisphere are heat waves and severe droughts associated with changes in general circulation. Here we analyze satellite data obtained by two different sounders, AIRS and TROPOMI. Different sensitivity to the lowest troposphere allows obtaining information about anthropogenic or pyrogenic contamination of the boundary layer. Shapes of areas polluted by mega-fires in 2019-2020 (Southeastern Australia) and 2021 (Central Siberia) coincide with the areas occupied by coal deposits. The Siberian Lena and Tunguska coal basins are the two largest coal fields in the world. In 2021, their combined area accounted for 90% of fire CO emission from the entire Russian Federation. So strong fires have not observed in this area before. Under- and sub-ground coal combustion may be included into the list of wildfire fuels, at least their role for ignition should be admitted. Further research is needed to assess the importance of coal fires to global climate.

Keywords: wildfires; coal fires; carbon monoxide; remote sensing

1. Introduction

Forest fires are considered common and even positive phenomena; fires free forests from old trees and makes it possible for young trees to develop and absorb CO2. The greenhouse gases released by fires, primarily carbon dioxide, are therefore part of the natural global carbon cycle. The above, however, is only true in a stable climate. Under the influence of human activity, the climate is changing, for example, temperatures are rising, which leads to an increase in the intensity and number of droughts that facilitate fires [1]. The contribution of wildfires to the carbon balance may be increasing [2,3]. Carbon dioxide (CO_2) and methane (CH_4) add to anthropogenic emission. Rising CO_2+CH_4 concentrations increase temperature trend further, as a positive feedback [4].

In recent years, fires in Russian forests have become known as catastrophic: they span over vast areas, creating thick smoke that spreads to regions adjacent to the fires [5]. Moreover, longer living gaseous emissions from Siberian fires fill almost completely the extratropical latitudes of the Northern Hemisphere [6,7]. The 2021 fires in Yakutia (Sakha) and the Krasnoyarsk region of Russia attracted particular attention [8,9].

By a coal fire we mean the uncontrolled burning or smoldering of a coal seam [10]. Coal fires are nothing new. Since the 60s of the last century, coal seams have been constantly burning near the city of Centralia in eastern Pennsylvania, USA [11]. Attempts to extinguish this fire were unsuccessful, and residents were forced to leave the city. The most famous fire in the World is the so-called "Burning Mountain" in south-eastern Australia [12]. The underground fire there is believed to be smoldering at a depth of about 30 m and has been going on for the last 6,000 years. Coal fires are reported from China, India, USA, Australia, Indonesia, Venezuela, South Africa, Russia, Croatia and other countries ([10] and references therein). The fires of this type can start from spontaneous combustion or from human exposure. The reaction of carbon in coal with oxygen in the air is an exothermic process that releases heat as carbon and oxygen react to form CO_2, CO and a variety

 doi:10.20944/preprints202312.1791.v1

of other products [12]. Coal fires have been known to burn for hundreds of years and date back to the Pleistocene [13].

Remote sensing research on coal fires mainly focuses on detecting thermal anomalies associated with coal combustion, detecting land cover changes under mining conditions, detecting land surface subsidence due to volume loss underground, and developing methods to identify risk areas for coal fires [11]. In addition, in-depth thermal analysis such as subpixel thermal mapping, emissivity-based geological mapping, and coal fire quantification have been conducted [14].

Remote measurements of CO_2 from satellites require extremely high precision. For CO these requirements are dramatically softer. Let's compare satellite measurements of CO and CO_2 in wildfires. The percentage change in concentration caused by the fire is mostly important. For example, the catastrophic fires in Indonesia in 2015 resulted in an increase in average whole-atmosphere CO_2 concentration of 2 ppm (2000 ppb) from a background concentration (outside the fire zone) of ~400 ppm [15]. Thus, the impact of fire is only 0.5%. This value is close to accuracy of the most advanced satellite CO_2 instrument OCO-2 (0.3% or ~1 ppm) [15]. Fires of similar intensity in Yakutia in 2021, according to the AIRS satellite sounder (see below), led to an increase in the monthly Xco to 160–170 ppb. For the same fire the more accurate TROPOMI (see Section 3.5 for abbreviations) sounder detected an increase up to 200 ppb with a background value for CO of just ~80 ppb. Therefore, fire signal for CO amounts to 100-200% whilst CO_2 increase is only 0.5%.

There is a large number of studies of CO emissions from wildfires based on measurements of CO from satellites based on data from TIR instruments (4.6 μm of wavelength) [16,17] , The weak point of TIR technique is a low sensitivity to the surface layers of the atmosphere. Significant progress in this area was achieved in 2017 with the launch into orbit of the Sentinel-5p satellite equipped with the TROPOMI SWIR sounder. A set of publications devoted to analysis of TROPOMI data for wildfires appeared on last four years [18–22]. Combination of TROPOMI CO measurements with an approach that uses satellite-observed fire radiative power (FRP) as proxy for fuel availability was examined by [23].

The main goals of this article is to demonstrate the capabilities of TROPOMI for studying pollution in the low troposphere and relationships between coal and forest fires. Also estimates for CO fire emission from the extra-tropical latitudes of the NH, updated to present time, are reported.

2. Materials and Methods

TROPOMI is an imaging spectrometer on the ESA Sentinel-5 Precursor platform in orbit at 824 km altitude. Its 2600 km swath provides global daily coverage at very high spatial resolution ,of 7.2 × 7.2 km^2 at nadir [24] I It measures radiation in the ultraviolet, visible and shortwave infrared spectra. Total CO column (TC) values, expressed in mol/m^2 and converted into Xco, column-averaged volumetric mixing ratio, were obtained from measurements of reflected solar SWIR radiation in the first overtone of the CO fundamental band in the spectral range of 2.3 μm [25]. Over land Xco were retrieved from solar radiance for clear sky and cloudy conditions. Measurements of CO over water are possible only when clouds are in the field of view [25]. Otherwise, due to the low reflectivity of open water in the SWIR range, the spectra of reflected light are too noisy. A special procedure is applied to estimate the fractional CO column below the cloud top [25]. A priori profiles are generated using the global chemical transport model TM5 [26]. The profiles vary by place, month and year.

AIRS is a diffraction grating spectrometer launched into a sun-synchronous polar orbit in May 2002 on board the Aqua satellite [27]. The instrument has a mirror scanning ±48.3° from nadir across the orbit. It provides nearly complete global daily coverage. The spectral resolution is 1.79 cm^{-1} in the fundamental absorption band of CO in the wavelength region of 4.6 μm. The instrument has a spatial resolution of 13.5 km at nadir. Currently (December 2023) AIRS is still operational. Monthly and daily average "AIRS-only" VMR profiles (version 7, level 3 [28]) for the period October 2002 to November 2023 for ascending orbits are available online in a 1° × 1° latitude-longitude grid at https://disc.gsfc.nasa . gov /datasets/ (accessed December 10, 2023), AIRS3STM_7.0 (monthly), and

 doi:10.20944/preprints202312.1791.v1

AIRS3STD_7.0. (daily). Xco were calculated as weighted averages of CO VMR values as a function of pressure for 24 layers of different thicknesses, used as weighting factors.

This article is based on two remote sensing experimental data sets. A comprehensive validation of the TROPOMI/Centinnel-5p TC-averaged mixing ratio of carbon monoxide and methane (Xco and Xch4) has been published [29]. 28 ground-based TCCON and 24 NDACC stations, included in that study, were located mostly in remote areas and characterize background concentrations of greenhouse gases. The stations were equipped with Fourier Transform interferometers of high spectral resolution. A system of mirrors tracked the Sun. The data were available only for clear sky conditions. Excellent agreement between TC-averaged mixing ratios of gases measured from the satellite and from the ground was documented.

AIRS Xco were validated by comparison with data from 9 TCCON sites [7]. These comparisons reveal a significant scatter of points and underestimation of AIRS' Xco. Appendix A). The mean slope of linear regression line was found to be 0.73, and the standard deviation for the slopes was estimated as ± 19%. The measured HNH anomalies of CO burden were corrected accordingly. The low Xco for AIRS are explained by reduced sensitivity of the retrieval algorithm to lower atmospheric altitudes. The AIRS sensitivity to the middle layers, namely 3-5 km of altitude, was verified by comparisons with aircraft CO in situ data in this range of altitude from 32 sites in USA and Canada (6905 profiles) [30] (Figure A2). A significant scatter for measurement days > 10 ppb was found. On average the binned values of AIRS Xco differed from the in situ aircraft data by less than 10 ppb within an Xco range of 90 to 140 ppb.

3. Results

3.1. Two decades of wildfire emissions.

Monthly and yearly CO emissions from wildfires in the HNH were calculated by [7] using a two-box (0 - 30 N and 30 - 90 N) mass balance model for the period between January 2003 and December 2021 (for model description see [16,17]). In 2021 a record high annual emission of 149 Tg CO yr^{-1} was found. This calculation was updated here using the same algorithm until October 2023 (Figure 1). The Global Fire Emission Database, version 4c (GFED4c, described by [31]) specified even a higher magnitude for 2021: 192 Tg CO yr^{-1} [7]. The plot of Figure 1 represents cumulative CO mass emitted in the HNH from the beginning of the given year. 2003, 2012, 2021 and 2023 were the years of "mega-fires". Figure 1 clearly demonstrates also a range of year-to-year variability of CO annual emissions for the "normal" fires. The time series of CO annual emissions is shown in Appendix B (Figure A3). A (5.1 ± 2.8) % yr^{-1} up-going trend for "normal" years was observed

The design of our box model does not allow to derive spatial distribution of emission inside the selected box. On the contrary, GFED4c approach provides global maps of CO fire emissions since 1997 with time resolution of one month. We used these maps to illustrate temporal variations of CO discharge from wildfires for various areas in the Russian Federation (Figure 2). Emission from Central Siberian forest/tundra domain (for boundaries see maps of Figure 3d and Figure A4) was compared with that from the rest of boreal Russia after 1997. The most striking feature of this plot is growing CO emission at the Central Siberia, especially after 2015 and up to maximum in 2021. In that year a contribution of the Central Siberia reached ~ 90% of total Russian pyrogenic CO output. Before 2015 emissions from that area for the most of previous period (12 years of total 19) were insignificant. Anthropogenic CO production in Russian Federation is in the range between 25 and 30 Tg CO yr^{-1} [32] , i.e. it is comparable with those from normal fires or lower than CO discharge from mega-fires.

Preprints (www.preprints.org) | NOT PEER-REVIEWED | Posted: 25 December 2023 doi:10.20944/preprints202312.1791.v1

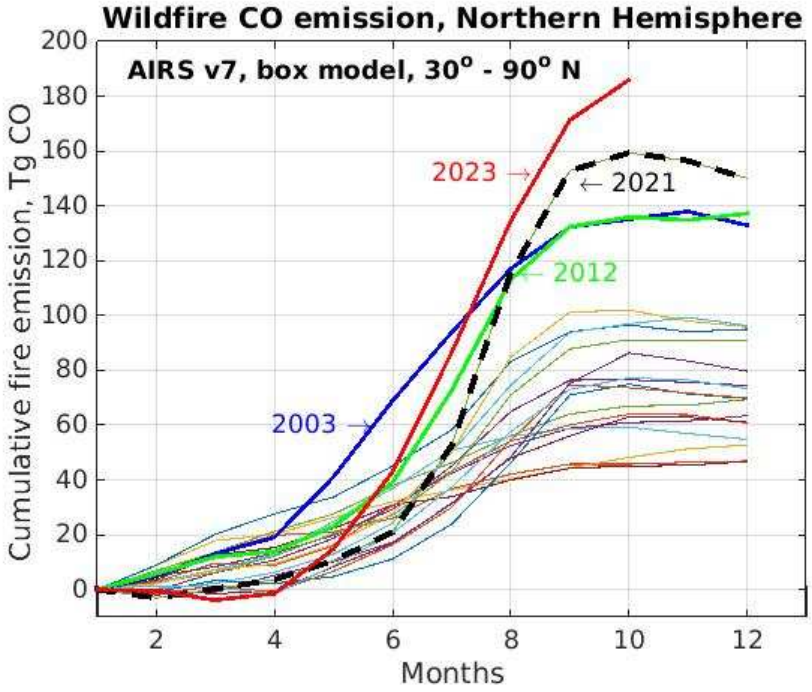

Figure 1. Cumulative CO monthly emission for HNH. 2003-2023. Mega-fires are indicated, yearly emissions are in the range of 140-180 Tg CO. Normal fires emit between 50 and 100 Tg CO per year.

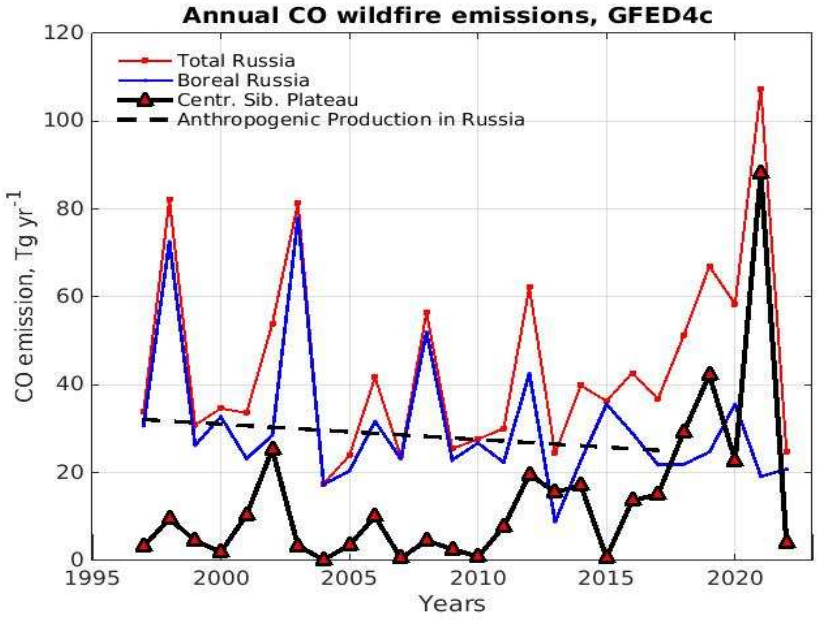

Figure 2. Wildfires CO annual emissions from Russia as derived from GFED4c [31] maps. Central Siberian plateau area corresponds to 3c. Boreal Russia dataset was calculated as a difference between Total Russia and Central Siberia.

Preprints (www.preprints.org) | NOT PEER-REVIEWED | Posted: 25 December 2023 doi:10.20944/preprints202312.1791.v1

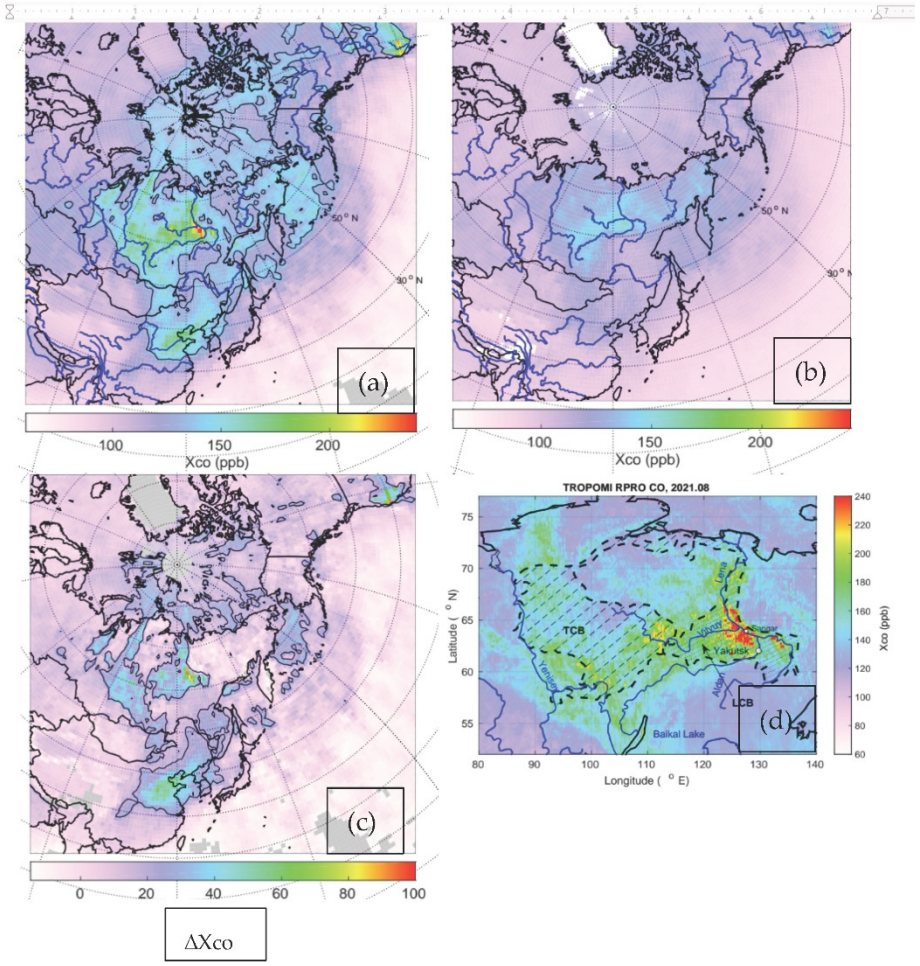

Figure 3. Monthly 1°x1° lat/lon maps of Xco in August, 2021, measured by TROPOMI (a), AIRS (b) and differential between them (c). Isolines in (c) correspond to ΔXco = 20 ppb. (d) is a zoom in of (a), but resolution is 0.25°x0.25°. Boundaries of Lena and Tunguska coal basins are shown by dash lines.

3.2. Mega-fire in Central Siberia in 2021 as seen remotely by TROPOMI and AIRS.

In this and the next sections CO measurements provided by two satellite-borne sounders for fire regions will be analyzed. Shortcomings of TIR and SWIR techniques will be discussed below in the Section 4.1. Geometry and spectroscopy of these two instruments are different. The TROPOMI registers Solar SWIR radiation penetrating the total atmospheric column and reflected by the surface. CO spectral features allow to calculate total number of CO molecules along this track. Dividing this number by the number of air molecules (excluding water vapor molecules) on the same way gives us total-column-average Volume Mixing Ratio (VMR), measured in parts per billion (ppb), usually denoted as Xco. The optical path can be shorter or longer depending on cloudiness and aerosol multiple scattering. The problem of accurate determination of the optical path is a central one for any SWIR or visible solar technique.

The AIRS grating spectrometer measures spectrally resolved Thermal IR (TIR) outgoing terrestrial radiation. The initial source of this radiation is the Earth surface, on the way to the satellite the radiation is absorbed and re-emitted by CO. The shape of absorption/emission spectral lines depends on air pressure and air temperature. They are different for different altitudes. A vertical profile of CO VMR for any location on the Globe and any time may be retrieved. A special complicated mathematical algorithm for solving this problem (called inverse problem) is applied. A significant drawback of the TIR approach is a dependence of the sensitivity on the atmospheric temperature profile: as a result, the sensitivity to CO in the lowest atmospheric layer diminishes. On the contrary, the sensitivity of SWIR techniques to all altitudes is almost the same for clear sky. This

 doi:10.20944/preprints202312.1791.v1

difference in sensitivity opens a door to separate TC-averaged (Xco) and low tropospheric (ideally, boundary layer) VMR. The latter is highly important for investigation of wildfires, namely to distinguish between flaring and smoldering types of burning. The shortcomings of the specific datasets, however, will be discussed below.

Emission of CO from the Siberian 2021 fire maximized in July and August. Monthly August Xco measured by TROPOMI and AIRS (Figure 3 a and b, respectively) have similarities and differences. Both sounders registered increased Xco over Central Siberia domain bounded by the rivers Yenisey (on the West) and Lena (on the East). TROPOMI's Xco for this area exceeds that measured by AIRS. Both instruments measured similar levels of Xco over the Pacific ocean and areas beyond East and/or Central Siberia. Pyrogenic CO from Siberia was transported northward and polluted the Arctic ocean area and the Bering sea. TROPOMI clearly "see" the polluted area in China.

Figure 3c displays the differential between these two data sets (TROPOMI minus AIRS). The ΔXco varies between ~0 and 100 ppb. If ΔXco = 0, then it means lowest pollution cases. In other words, real CO profile does not differ from a priori one. The a priori is obtained from a cluster of available aircraft and surface in situ measurements for unperturbed atmosphere. Therefore, ΔXco can be treated as a measure for deviation of lower tropospheric VMR from a priori. Mostly important is a character of emission mechanism. Urban emissions are connected with low-temperature processes. Flaring wildfires, on the contrary, generate very hot burning products that are mixed throughout the atmospheric column effectively and easily reach the altitudes of several kilometers. Intermediate examples are smoldering peat and coal fires. Using TIR and SWIR remote sensing is promising for elucidation of the fire's nature. Shortcomings of the current versions of retrieval techniques will be discussed in the Section 4.

The map of Figure 3d is a zoom-in of Figure 3a. It illustrates a general similarity in the shape of enhanced Xco area and locations of two coal basins, Tunguska (TCB) and Lena (LCB). Maximal monthly average Xco (up to 240 ppb) were recorded by TROPOMI to the North of Yakutsk (the capital of the Sakha Republic) near the small settlement Sangar. An underground coal fire there began in May, 2000, it has not been extinguished by 2011 [33]. Citizens of Sangar suffer pollution from this fire year-round still now [34].

3.3. Mega-fire in Australia in 2019/2020.

The summer season of 2019/2020 was characterized by record severe wildfires in Australia [35]. Figure 4, similarly to Figure 3, displays Xco for January, 2020, provided by two sensors, together with a differential between them. The color scale for Figure 4, a and b, is from 40 ppb to 160 ppb, slightly different from that for Figure 3 (CO background concentration in the Southern hemisphere is lower than in Northern). The color scale for Figure 4c is between -10 and 100 ppb, i.e., the same as for Siberia. A plume of fire products, including CO, stretched across the Pacific Ocean until South America's shore. Origin of the plume was in South-Eastern Australia near Sydney city. These three maps (Figure 4, a, b, and c) evidence in favor of CO eastward transfer through the lowermost atmospheric layers. Figure 4d is a map of individual TROPOMI retrievals (pixels) for December 30, 2019. The burning area coincided with the shape of the Sydney coal Basin.

Preprints (www.preprints.org) | NOT PEER-REVIEWED | Posted: 25 December 2023 doi:10.20944/preprints202312.1791.v1

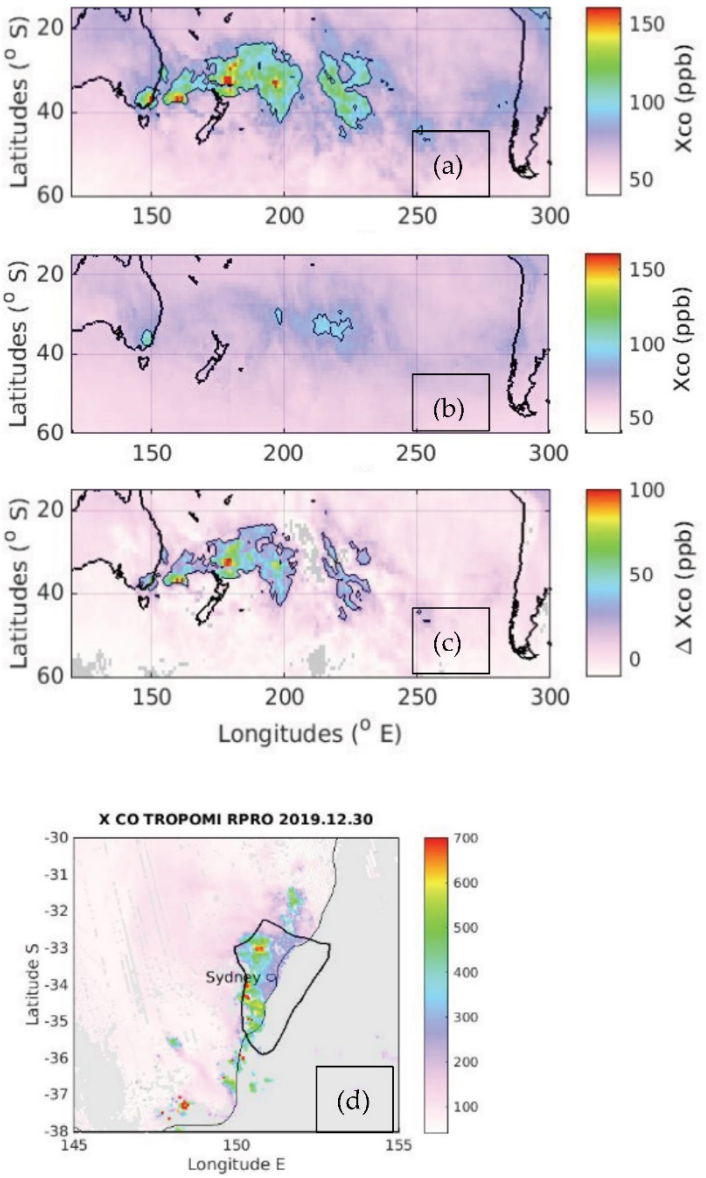

Figure 4. The same as Figure 3, but for January 2020, Australia; (c) is a map of immediate TROPOMI pixels for December 30, 2019, a contour of the Sydney Coal Basin is shown in black line.

3.4. Abbreviations

TROPOMI: . TROPOspheric Monitoring Instrument
AIRS Atmospheric InfraRed Sounder
TCCON: Total Carbon Column Observing Network
NDACC: Network for the Detection of Atmospheric Composition Change
HNH: High Northern Hemispheres
TCB: Tunguska Coal Basin
LCB: Lena Coal Basin
NOAA: National Oceanic and Atmospheric Administration
SWIR: Short-Wave InfraRed
TIR: Thermal InfraRed
OCO-2: Orbiting Carbon Observatory-2
ESA: European Space Agency
VMR: mixing ratio by volume

 doi:10.20944/preprints202312.1791.v1

4. Discussion

4.1. Evaluation of TROPOMI database for fire investigation

As it was mentioned in the section 2, the current version of TROPOMI CO land data make use pixels for all atmospheric conditions: from clear sky (maximum sensitivity to low troposphere) to overcast (zero sensitivity). The data were validated by comparison with Fourier Transform solar-tracking interferometers, i.e. just for clear sky conditions (Figure A1). These data are very helpful, but remote sensing of CO for cloudy days over land were not validated at all. Dense smoke in fire plumes complicates the analysis by a necessity to take multiple scattering into account. The Xco data reported for the marine surface are even in a worth position: no information for clear sky can be retrieved due to extremely low reflectivity of water surface in the SWIR region. The only rare geometry when it is possible is a mirror-like reflection (glint).

Monthly mean Xco maps reported here (Figs 3 and 4) qualitatively evidence much better performance of TROPOMI for wildfires than that of AIRS. TROPOMI clearly locates the fire sources and allows further investigation of this phenomenon. An improvement of this technique to take into account vertical sensitivity for each pixel to provide more quantitative data is feasible.

Coupling of a SWIR and a TIR sounder to distinguish between low tropospheric and mid tropospheric pollutions, like that, was realized for a TROPOMI-MOPITT pair [22]. The approach used in this paper (simple differential ΔXco provided by two sensors) is preliminary. Algorythms of this sort should use averaging kernels (a measure of sensitivity) and a priori CO profiles (derived from pools of available in situ measurements and/or modeling results) for each pixel. Ideally, a special "hybrid" algorithm that would produce Xco for total column, mid altitudes and low altitudes from spectral radiances (Level 1) measured by SWIR and TIR sensors may be developed. So, the maps of Figure 3c and Figure 4c should be considered just qualitative. This is particularly true for marine areas where TROPOMI data are insensitive to sub-cloud air beyond glint cases.

4.2. Role of coal burning in Siberian and Australian fires

Available trend estimates from inventories based on bottom-up or making use of a combination of bottom-up and top-down information [23] are controversial. Global CO fire emissions seem to have no significant positive trend or even show a decrease during 2003-2021. Certain regions, nonetheless, see increasing emissions, e.g., Australia or temperate North America. These inventories consider 18 types of fuels; underground coal is not included as such for wildfires.

Figure 2 clearly evidence a growing trend of CO emission from central Siberia and relatively stable pattern for the rest of Russia (mostly southern Siberian and Far Eastern Russia taiga, see a map in the Appendix D). The shape of polluted area in 2021 coincides with the locations of two coal basins (Figure 3d). The co-location of wildfires and coal deposits in Siberia and Australia (Figure 4d) is unlikely to be accidental.

The Tunguska Coal Basin, Russia (coal reserves - 2.299 trillion tons with area of more than a million km2) [36] and the Lena Coal Basin, Russia (1.647 trillion tons; 0.75 million km2) [37] are the two greatest coal fields in the World . The severe wildfires in New South Wales, Australia in 2019/2020 occurred inside boundaries of the Sydney Coal Basin (20 million tons of coal; area 44,000 km2 onshore plus 5,000 km2 offshore) [35].

It is quite natural to assume a significant role of coal fires for ignition of forest fire. The Sangar coal fire [33,34] most probably ignited fire in Yakutia (LCB area in Figure 3d). A reverse ignition of underground coal by severe forest fires is questionable. This effect is not investigated and presently may be considered just a speculative opportunity.

It is quite interesting that catastrophic coal fires in the geological past have been assumed for this area already. The mass extinction of biological species at the boundary of the Permian and Triassic periods 252 million years before the present was a major environmental catastrophe, leading to a radical restructuring of marine and continental communities. [36,38,39]. Today, most experts [36,40] have no doubt that the main cause of the crisis was trap volcanism - a huge surge of volcanic activity in the territory of what is now central Siberia (which, like almost all the rest of the land, was

Preprints (www.preprints.org) | NOT PEER-REVIEWED | Posted: 25 December 2023 doi:10.20944/preprints202312.1791.v1

then part of the single continent of Pangea). According to paleoclimatic studies [39], Siberian coal and forest fires, in combination with seafloor methane emissions from clathrates and volcanic CO2, have caused extreme global warming of 5-9°C, leading to the Great Permian Extinction.

A similar effect is impossible now and in the near future: volcanic activity, which was the main cause of coal fires at that time, is highly unfeasible. However, we cannot exclude a "lite" version of this scenario, in which the main trigger for forest and coal fires would be anthropogenic impact via change in circulation and droughts. Warming climate may induce intensification of coal fires. Coal burning should be included as an immediate component of global wildfires. The vast carbon reserves, stored in Siberia, appear to pose a persistent climatic risk for the rest of XXI century.

Funding: This research received no external funding

Data Availability Statement: AIRS datasets: AIRS3STM_7.0, AIRS3STD_7.0 https://disc.gsfc.nasa.gov/datasets/. GFED4: https://www.geo.vu.nl/~gwerf/GFED/GFED4/. TCCON: https://data.caltech.edu/records/20140.

Acknowledgments: In this section, you can acknowledge any support given which is not covered by the author contribution or funding sections. This may include administrative and technical support, or donations in kind (e.g., materials used for experiments).

Conflicts of Interest: The authors declare no conflict of interest.

Appendix A

Validation of satellite databases

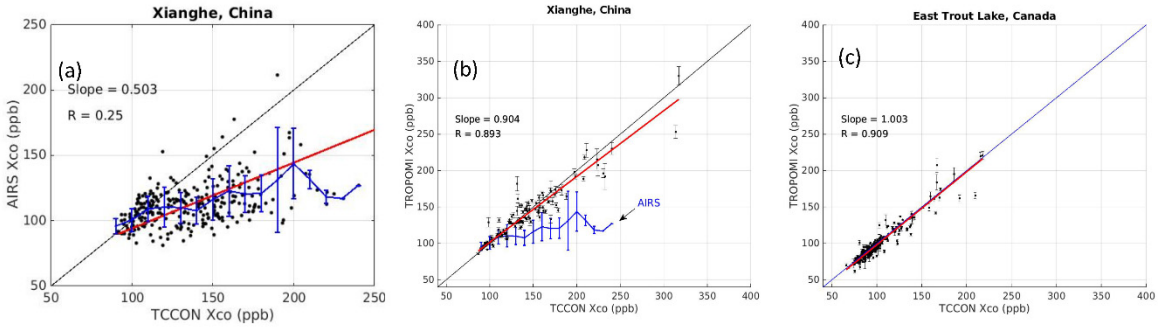

Figure A1. Comparison of satellite-borne and surface CO TCCON measurements. (a) TCCON site in China, AIRS, black points are daily mean Xco; blue line is for binned data points. error bars for standard deviations (STD). (b) The same site, but for TROPOMI; blue line is moved from (a). (c) TCCON site in Canada, boreal forest, TROPOMI.

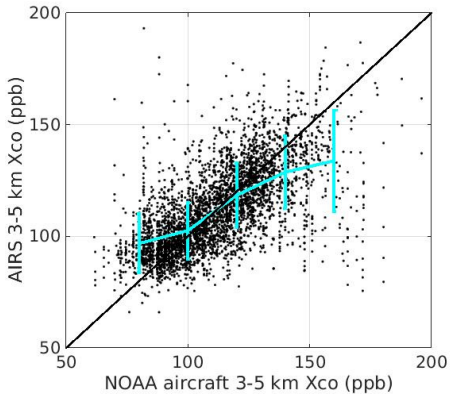

Figure A2. Comparison of AIRS daily mean Xco for the 3-5 km range of altitudes with data measured in situ on an aircraft. Blue line and error bars are for binned means and STD.

Preprints (www.preprints.org) | NOT PEER-REVIEWED | Posted: 25 December 2023 doi:10.20944/preprints202312.1791.v1

Appendix B

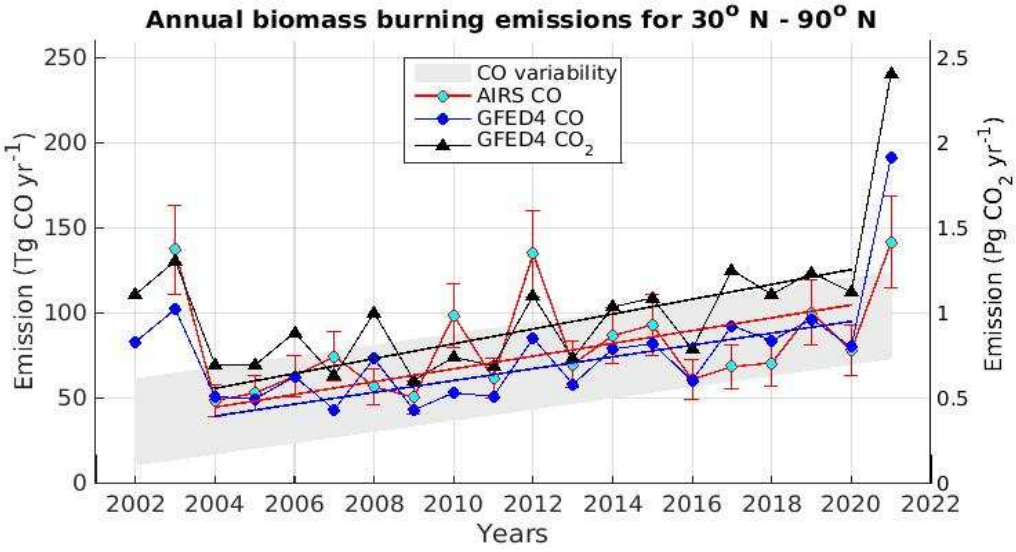

Figure A3. Annual CO emitted by fires in HNH according to AIRS data and GFED4c estimates [7]. CO_2 emission (right scale) is plotted for comparison. Least squares regression lines are shown as well. Error bars follow from validation and estimated as ±19%. Shaded area corresponds to GFED4 CO ± 2 STD (standard deviation) of the yearly points.

Appendix C

Figure A4. Locations of coal basins in Russia. (courtesy https://vovru.ru/География_8_класс_Алексеев/41.2.jpg) Green ellipse indicates location of Southern Siberian taiga. Thick blue dash line is an approximate southern boundary of the permafrost zone.

References

1. Stocks, B.J.; Fosberg, M.A.; Lynham, T.J.; Mearns, L.; Wotton, B.M.; Yang, Q.; Jin, J-Z;, Lawrence, K.; Hartley, G.R.; Mason, J.A. ; McKenney, D.W.. Climate change and forest fire potential in Russian and Canadian boreal forests. Clim. Change 1998, 38, 1–13.
2. Kasischke, E; Stocks, B. Fire, climate change, and carbon cycling in the boreal forest; Springer-Verlag: New York, NY, USA, 2000; 461 p.
3. Seiler, W.; Crutzen, P.J. Estimates of gross and net fluxes of carbon between the biosphere and the atmosphere from biomass burning. Clim. Change 1980, 2, 207–247.
4. Cochrane, M. A.; Alencar, A.; Schulze, M. D.; Souza C. M.; Nepstad, D. C.; Lefebvre, P.; Davidson, E. A. Positive Feedbacks in the Fire Dynamic of Closed Canopy Tropical Forests Science. 1999, 284, 1832-1835.
5. Romanov, A.A.; Tamarovskaya, A.N.; Gusev, B.A.; Leonenko, E. V.; Vasiliev, A.S., Krikunov, E.E. Catastrophic PM2.5 emissions from Siberian forest fires: Impacting factors analysis. Environ. Pollut. 2022, 119324, doi:10.1016/j.envpol.2022.119324.
6. Romanov, A.A.; Tamarovskaya, A.N.; Gloor, E.; Brienen, R.; Gusev, B.A.; Leonenko, E. V.; Vasiliev, A.S.; Krikunov, E.E.. Reassessment of carbon emissions from fires and a new estimate of net carbon uptake in Russian forests in 2001–2021. Sci. Total Environ. 2022, 157322 , doi:10.1016/j.scitotenv.2022.157322.
7. Yurganov, L.; Rakitin, V. Two Decades of Satellite Observations of Carbon Monoxide Confirm the Increase in Northern Hemispheric Wildfires. Atmosphere (Basel). 2022.13(9): 1–12. doi:10.3390/atmos1309147
8. Ponomarev, E.; Zabrodin, A.; Ponomareva, T. Classification of Fire Damage to Boreal Forests of Siberia in 2021based on the dNBR Index. Fire. 2022, 5, 19. https://doi.org/10.3390/fire5010019
9. Bondur, V.G.; Gordo, K.A.; Voronova, O.S.; Zima, A.L.; Feoktistova, N.V. Intense Wildfires in Russia over a 22-Year Period According to Satellite Data. Fire. 2023, 6, 99. https://doi.org/10.3390/fire60300991.5
10. Dijk, P.; Zhang, J.; Jun, W.; Kuenzer, C.; Wolf, K. H. A. A. Assessment of the contribution of in-situ combustion of coal to greenhouse gas emission; based on a comparison of Chinese mining information to previous remote sensing estimates. International Journal of Coal Geology. 2011, 86(1), 108-119. https://doi.org/doi:10.1016/j.coal.2011.01.009
11. Elick, J. M. Mapping the coal fire at Centralia, Pa using thermal infrared imagery: International Journal of Coal Geology. 2011, 87, p. 197-203. https://doi.org/10.1016/j.coal.2011.06.018
12. Ellyett, C. D. ; Fleming, A. W. Thermal infrared imagery of The Burning Mountain coal fire Remote Sensing of Environment, 1974, 3(1), 79-86 DOI: 10.1016/0034-4257(74)90040-6
13. Zhang, X.M.; Kroonenberg, S.B. ; de Boer, C.B. Dating of coal fires in Xinjiang, north-west China. Terra Nova, 2004, 16(2), 68 - 74.
14. Zhang ,X. ; Zhang, J. ; Kuenzer C.; Voigt, S. ; Wagner, W. Capability evaluation of 3–5 μm and 8–12.5 μm airborne thermal data for underground coal fire detection , Int. J. Rem. Sensing, 2004, 25(12), 2245-2258, DOI: 10.1080/01431160310001618112
15. Crisp, D.; Johnson, The orbiting carbon observatory mission. Acta Astronautica, 2005, 56(1–2), 193-197.
16. Yurganov, L. N.; Duchatelet, P.; Dzhola, A. V.; Edwards, D. P.;Hase, F.; Kramer, I.; Mahieu, E.; Mellqvist, J.; Notholt, J.; Novelli, P. C.; Rockmann, et al. .: Increased Northern Hemispheric carbon monoxide burden in the troposphere in 2002 and 2003 detected from the ground and from space. Atmos. Chem.Phys., 2005, 5, 563–573, doi:10.5194/acp-5-563-2005,.
17. Yurganov, L. N.; Blumenstock, T.; Grechko, E. I.; Hase, F.; Hyer,E. J.; Kasischke, E. S.; Koike, M.; Kondo, Y.; Kramer, I.; Le-ung, F.-Y., et al. A quantitative assessment of the 1998 carbon monoxide emission anomaly in the northern Hemisphere based on total column and surface concentration measurements. J. Geophys. Res., 2004. 109, D15305, doi:10.1029/2004JD004559,.
18. Magro, C.; Nunes, L.; Gonçalves, O. C.; Neng, N. R.; Nogueira, J. M. F.; Rego, F. C.; Vieira, P. Atmospheric trends of CO and CH4 from extreme wildfires in Portugal using sentinel-5P TROPOMI level-2 data. Fire, 2021, 4(2), 25. https://doi.org/10.3390/fire4020025
19. Wan, N.; Xiong, X.; Kluitenberg, G. J.; Hutchinson, J. M. S.; Aiken, R.; Zhao, H.; Lin, X. Estimation of biomass burning emission of NO2 and CO from 2019–2020 Australia fires based on satellite observations. Atmos. Chem. Phys., 2023, 23, 711–724, https://doi.org/10.5194/acp-23-711-2023.
20. van der Velde, I. R.; van der Werf, G. R.; Houweling, S.; Eskes, H. J.; Veefkind, J. P.; Borsdorff, T.; Aben, I. Biomass burning combustion efficiency observed from space using measurements of CO and NO2 by the TROPOspheric Monitoring Instrument (TROPOMI), Atmos. Chem. Phys., 2021, 21, 597–616, https://doi.org/10.5194/acp-21-597-2021,.
21. Wang, Y.; Zhang, Y.; Zhao, C.; Dong, D.; Wang, K. CO and CH4 atmospheric trends from dense multi-point forest fires around the city of Chongqing using spaceborne spectrometer data. Atmospheric Pollution Research 2023, 14, 101807.

22. Martínez-Alonso, S.; Deeter, M.; Worden, H.; Borsdorff, T.; Aben, I.; Commane, R.; Daube, B.; Francis, G.; George, M.; Landgraf, J.; Mao, D.; McKain, K.; Wofsy, S. 1.5 years of TROPOMI CO measurements: comparisons to MOPITT and ATom, Atmos. Meas. Tech., 2020 ,13, 4841–4864, https://doi.org/10.5194/amt-13-4841-2020,.
23. Griffin, D.; Chen, J.; Anderson, K.; Makar, P.; McLinden, C. A.; Dammers, E.; Fogal, A. Towards an improved understanding of wildfire CO emissions: a satellite remote-sensing perspective, EGUsphere [preprint], ,2023, https://doi.org/10.5194/egusphere-2023-649, 2023.
24. Veefkind, J.P.; Aben, I.; McMullan, K.; Förster, H.; de Vries, J.; Otter, G.; Claas, J.; Eskes, H.J.; de Haan, J.F.; Kleipool, Q.; et al. TROPOMI on the ESA Sentinel-5 precursor: a GMES mission for global observations of the atmospheric composition for climate, air quality and ozone layer applications. Remote Sens. Environ., 2012, 120, 70–83. doi: 10.1016/j.rse.2011.09.027.
25. Landgraf, J.; van de Brugh, J.; Scheepmaker, R.; Borsdorff, T.; Hu, H.; Houweling, S.; Butz, A.; Aben, I.; and Hasekamp, O. Carbon monoxide total column retrievals from TROPOMI shortwave infrared measurements, Atmos. Meas. Tech., 2016, 9, 4955–4975, https://doi.org/10.5194/amt-9-4955-2016.
26. Krol, M.; Houweling, S.; Bregman, B.; van den Broek, M., Segers, A.; van Velthoven, P.; Peters, W.; Dentener, F.; Bergamaschi, P. The two-way nested global chemistry-transport zoom model TM5: algorithm and applications, Atmos. Chem. Phys., 2005, 5, 417– 432, doi:10.5194/acp-5-417-2005,.
27. Aumann, H. H. ; Chahine, M. T.; Gautier, C.; Goldberg M. D.; Kalnay,E.; McMillin, L. M.; Revercomb, H.P.; Rosenkranz, P.W.; Smith, W. L.; Staelin, D. H. et al. AIRS/AMSU/HSB on the Aqua mission: design, science objectives, data products and processing systems. IEEE Trans. Geosci. Rem. Sens. 2003, 41, 253-264.
28. AIRS project. Aqua/AIRS L3 Daily Standard Physical Retrieval (AIRS-only) 1 degree x 1 degree V7.0, Greenbelt, MD, USA, Goddard Earth Sciences Data and Information Services Center (GES DISC), https://doi.org/10.5067/UO3Q64CTTS1U (2019).
29. Sha, M. K.; Langerock, B.; Blavier, J.-F. L.; Blumenstock, T.; Borsdorff, T.; Buschmann, M.; Dehn, A., De Mazière, M.; Deutscher, N. M.; Feist, D. G. et al. Validation of methane and carbon monoxide from Sentinel-5 Precursor using TCCON and NDACC-IRWG stations, Atmos. Meas. Tech.,2021, 14, 6249–6304, https://doi.org/10.5194/amt-14-6249-2021,.
30. McKain, K.; Sweeney, C.; Baier, B.; Crotwell, A.; Crotwell, M.; Handley, P.; Higgs, J.; Legard, T.; Madronich, M.; Miller, J. B.; et al. .. NOAA Global Greenhouse Gas Reference Network Flask-Air PFP Sample Measurements of CO2, CH4, CO, N2O, H2, SF6 and isotopic ratios collected from aircraft vertical profiles [Data set]. Version: 2023-08-23. 2023. https://doi.org/10.15138/39HR-9N34
31. van der Werf, G. R.; Randerson, J. T.; Giglio, L.; van Leeuwen, T. T.; Chen, Y.; Rogers, B. M.; Mu, M; van Marle, M. J. E.; Morton, D. C.; et al. Global fire emissions estimates during 1997–2016. 2017 Earth Syst. Sci. Data, 9, 697–720 .
32. Crippa, M.; Guizzardi, D.; Butler, T.; Keating, T.; Wu, R.; Kaminski, J.; Kuenen, J.; Kurokawa, J.; Chatani, S.; Morikawa, T. et al. The HTAP_v3 emission mosaic: merging regional and global monthly emissions (2000–2018) to support air quality modeling and policies, Earth Syst. Sci. Data, 2023. 15, 2667–2694, doi:10.5194/essd-15-2667-2023.
33. Chemezov E. N. Localization of an underground fire at the sangarskaya mine (*Локализация подземного пожара на шахте «Сангарская»*) Mining informational and analytical bulletin. 2011. №12, 196-197, ISSN 0236-1493 https://giab-online.ru/en/catalog/archives/10582/view
34. Ivanova N. Eternal flames of Sangar: 20 years of life on a powder keg. 2021. https://dobro.press/blogi/vechnye-ogni-sangara-20-let-zhizni-na-porohovoi-bochke (in Russian)
35. Clarke, H.; Cirulis, B.; Penman, T. et al. The 2019–2020 Australian forest fires are a harbinger of decreased prescribed burning effectiveness under rising extreme conditions. Sci Rep. 2022. 12, 11871 . https://doi.org/10.1038/s41598-022-15262-y
36. Davydov, V.I. Tunguska Coals, Siberian Sills and the Permian-Triassic Extinction. Earth-Science Reviews 2021, 212, 103438. https://doi.org/10.1016/j.earscirev.2020.103438
37. Ignatchenko, N. A. Geologicheskoe stroenie i ugol'nye mestorozhdeniia zapadnoi chasti Lenskogo ugol'nogo basseina. 1960. Moscow, (In Russian). https://encyclopedia2.thefreedictionary.com/Lena+Coal+Basin

38. Payne, J. L.; Clapham, M. E. End-Permian Mass Extinction in the Oceans: An Ancient Analog for the Twenty-First Century? Annual Review of Earth and Planetary Sciences. 2012, 40, 89-111 .
39. Elkins-Tanton,L. T.; Grasby, S. E.; Black, B. A.; Veselovskiy, R. V.; Ardakani, O. H.; Goodarzi, F. Field evidence for coal combustion links the 252 Ma Siberian Traps with global carbon disruption. Geology. 2020. 48, 986–991. DOI: 10.1130/G47365.1.
40. Burgess, S.D.; Bowring, S.; Shen SZ. High-precision timeline for Earth's most severe extinction. Proc Natl Acad Sci U S A. 2014 ;111(9), 3316-3321. doi: 10.1073/pnas.1317692111. Epub 2014 . Erratum in: Proc Natl Acad Sci U S A. 2014 Apr 1;111(13):5060. PMID: 24516148; PMCID: PMC3948271